A big fan of signals? Exploring autogenic and allogenic process and product in a numerical stratigraphic forward model of submarine-fan development

Peter M. Burgess, Isabella Masiero, Stephan C. Toby, Robert A. Duller

Quantitative Experimental Stratigraphy Group, Jane Herdman Laboratory, Department of Earth, Ocean and Ecological Science, University of Liverpool, Brownlow Street, Liverpool L69 3GP, U.K.

Abstract

Distinguishing an allogenic signal from trends and patterns produced by autogenic processes is a critical element in interpreting, understanding, and predicting strata. Lobyte3D is a new reduced-complexity model of dispersive flow over an evolving topography on fan systems that produces surprisingly complex potentially hierarchical strata despite a simple formulation. Two submarine-fan model scenarios are run, one with constant sediment input, and one with a sinusoidal variation in sediment input with an oscillation period of 25 ky and a peak-to-trough 80% volume change. Both model scenarios show that flows cluster to produce lobes which migrate and can rapidly switch location. Runs tests that can detect thickening and thinning bed trends and spectral analysis that detects the frequency of any signal present suggest that strata can be ordered even in the absence of any allogenic signal, with cycles and trends in bed thickness, but no single characteristic frequency. In the oscillating-supply scenario, an allogenic signal is present in places, particularly in the axial mid fan, but may be difficult to distinguish from the autogenic signal with only limited outcrop data, and without knowing *a priori* how

the allogenic signal is likely to be preserved in complex and incomplete strata. Based on these limited model results we hypothesise that analysis of mid-fan vertical sections, using simple power-spectrum analysis and counting of the significant peaks present across a range of frequencies, may allow identification of a “signal bump” that could be evidence of the presence and nature of allocyclic forcing. Further Lobyte3D modelling work will explore if and how the “signal bump” is preserved with input signals across a range of frequencies and amplitudes, to guide further data collection and interpretation in outcrop and subsurface strata.

Introduction

A basic premise of much stratigraphic analysis is that an external signal (e.g., climatic oscillations) is often present in strata, and detectable through analysis of simple properties such as trends and patterns in bed thickness (Sinclair and Cowie, 2003; Burgess, 2006; Prelat and Hodgson, 2013; Talling, 2014). This is important because, if a signal is indeed detectable, strata represent a significant archive of climatic and tectonic history (Knight and Harrison, 2012). It also has important implications for prediction of stratal properties such as the spatial distribution of hydrocarbon reservoir rocks, since strata organized into patterns may be easier to predict (Mayall et al., 2006). Despite this potential importance, we still lack a detailed understanding of exactly how external forcing works to create stratal patterns identifiable in a one-dimensional vertical succession, and sometimes conclusions of forcing are based more on assumption than evidence (e.g., Gong et al., 2018). A better understanding of how patterns are recorded may make such patterns easier to detect, or perhaps better explain their absence (Burgess, 2016).

Submarine-fan strata may be particularly suitable to analyze for records of external (allogenic) change because deposition is largely aggradational, and significant stratigraphic surfaces are likely traceable over long distances, for example between outcrops (e.g., Straub and Pyles, 2012). Other geoscientists disagree, emphasizing evidence that submarine-fan strata are often disordered and essentially stochastic (Anderton, 1995). Debate persists because identification of allogenic signals from stratal patterns is often not straightforward from outcrop or subsurface data (e.g., Kim et al., 2014; Harris et al., 2016). Strata that record some cyclical autogenic process are also assumed to be more likely to show a pattern and organization (Hajek et al., 2012; Li et al., 2016). Therefore to unambiguously infer past climate or tectonic controls, allogenic order needs to be distinguishable from possible order associated with an autogenic signal.

Numerical stratigraphic forward modelling is a useful method to understand how stratal patterns form, and why they do not. Here we introduce Lobyte3D, a three-dimensional reduced-complexity numerical stratigraphic forward model, developed as a new component in a carbonate forward model CarboCAT (Burgess, 2013) and somewhat similar in formulation to other recent numerical models of submarine-fan systems (Teles et al., 2016; Groenenberg et al., 2010; Wang et al., 2017). We use Lobyte3D to explore how sediment accumulates on a submarine-fan surface in response to the morphodynamic feedback between depositional topography and flow routing (e.g., Reitz et al., 2010), either with or without periodic variation in the sediment supply to the fan, representing the presence and absence of an external signal respectively. We analyze bed thickness in one-dimensional vertical sections of strata, since this is a ubiquitous data type recovered from the stratigraphic record in both outcrop and subsurface studies, and therefore particularly important to understand more fully.

Methods

Summary of the Numerical Model Lobyte3D

Lobyte3D is a reduced-complexity model (Bokulich, 2013) that produces three-dimensional representations of fan strata (Figure 1A) using simple but logically consistent representations of various gravity-driven sediment transport mechanisms, for either siliciclastic or carbonate sediment. Source code for Lobyte3D is available in the data archive. Each Lobyte3D run consists of a specified number of time steps, with one or more flow events per time step, each producing what we refer to as a bed. Flow deposition is followed by deposition of a constant-per-time-step thickness of hemipelagic strata, which also form beds between successive flows, and often thicker beds deposited over several time steps when no flows are present. Each flow event is calculated as a geologically instantaneous process, with a repeat time between events, so that 1000 flows with a repeat time of 1000 years would represent 1 My of elapsed model time. With deposition on a simple bathymetry, flow bed thickness will correlate directly to input flow volume, allowing an external signal in the input flow volume to be preserved in the strata. However, spatial and temporal heterogeneity in deposited strata can arise from variations in flow routing.

Flow routing is sensitive to evolving topography, leading to interesting feedback behavior. Deposition of previous flows modifies and controls deposition of subsequent flows, in an autogenic lobe-switching process that can generate complex, heterogeneous strata in which external variations in sediment supply may be difficult to detect. Lobyte3D calculates transport and deposition on a simple orthogonal *x-y* grid. Model grid dimensions can vary but a typical configuration is a 20-by-20-km grid, with a cell size of 100 m. Any initial model topography can be used, but an appropriate example to generate realistic fan geometries is a homoclinal planar slope that passes down-dip to a flat basin-floor topography (Figure

1A). Each flow is introduced at a specified position on the edge of the model grid (Fig. 1A), with a specific flow volume that can be constant or variable through a model run.

Model Processes

The main processes represented by Lobyte3D are: 1) sediment supply from an external source, or weathering and erosion of subaerial model topography 2) confined, down-slope sediment transport and bypass processes, and 3) deposition of sediment from the dispersive, decelerating flows.

Sediment Supply, Sediment Source Area, and Erosion

Sediment supply into a Lobyte3D model is either specified as a volume of sediment introduced to the edge of the model ready for transport, or determined from topographic erosion calculated in Lobyte3D as a function of water volume input, water flow, and slope, at a rate proportional to a calculated stream-power index (Moore et al., 1991). In this work we use only the simpler method of specifying the sediment input introduced at a single point on the model grid margin.

Downslope Sediment Transport and Bypass

As a simplification of the stresses induced by fluid flows that control erosion and deposition, Lobyte3D uses flow velocity as a simple proxy to control sediment transport and deposition. Flow velocity is a function of topographic gradient and the flow thickness, and so long as the flow velocity exceeds a specified threshold for deposition, Lobyte3D moves all the sediment volume in one event downslope as one single packet of sediment in just one model grid cell at any time, following a steepest gradient descent down the slope (Figure 1B). Sediment transport starts from coordinates that determine the sediment source position on the model grid (Figure 1A). Flows can start from any position on the model grid, allowing flexibility modelling simple or complex sediment-input scenarios. Mean flow thickness H is calculated as a proportion of the total sediment volume transported by the gravity flow, assuming that higher flow volumes generate thicker flows. Calculation of the flow height also accounts for a run-up height (Kneller and Buckee, 2000), so that the elevation Z of the top of the flow is calculated as

$$Z = z_{x,y} + H + h_r \tag{1}$$

Where $z_{x,y}$ is the elevation of the cell where the flow is located, H is the flow thickness in meters, and h_r is the run-up height, also in meters. The run-up height has been defined by Kneller and Buckee (2000) as the maximum height that can be reached by a flow for a given velocity, allowing simplified approximation of the hydrodynamic pressure linked to flow kinetic energy, enabling the flow to overcome topographic barriers. Run-up-height is calculated as a function of flow velocity and then ”virtually” added to the flow height H, allowing the flow to flow over topographic obstacles that are equal, or higher than the flow median thickness. For homogeneous flows, according to Rothman et al. (1985), the run up height is given by

$$h_r = \frac{U^2}{2g} \tag{2}$$

where g is acceleration due to gravity. If the flow is submarine, the gravity force is reduced by buoyancy, so that

$$g' = g\left({}^{\rho_f}/_{\rho_w}\right) \tag{3}$$

where ρ_w is the density of water and ρ_f is the flow bulk density, which is the product of the grain density ρ_s and the volumetric sediment concentration C_v. Mean flow thickness remains constant during downslope transport, so this is a simplified treatment ignoring entrainment of sediment and fluid, but flow thickness is recalculated during flow deposition as the flow volume per cell decreases due to deposition and flow dispersion.

Flow height, including run-up height, is included in the calculation of flow routing. Flow routing uses a steepest descent algorithm such that the slope, S, and the mean velocity, U, between the current flow location and eight neighboring cells is calculated as

$$S = \frac{z_{i+y,j+x} - Z_{i,j}}{\Delta s} \qquad (rook's\ case) \tag{4}$$

for the perpendicular neighbors, and by

$$S = \frac{z_{i+y,j+x} - Z_{i,j}}{\sqrt{2\Delta s}} \qquad (bishop's\ case) \tag{5}$$

for diagonal cells, where Δs is the cell size in meters. The flow is routed down the steepest slope, into the lowest neighboring cell.

Mean flow velocity between cells is calculated by different methods depending on the flow type being represented, either a low-concentration or a high-concentration gravity flow. For low concentration flows we use a Chézy-type formula for steady, turbulent, open channel flow

$$U = \sqrt{\frac{8gC_v}{f(1+\alpha)}\,HS} \tag{6}$$

where f is the Darcy-Weisbach friction coefficient, ≈0.04, and α is an empirical coefficient ≈0.43. High-concentration gravity flows are best described using a resistance-to-flow relationship, using mean flow velocity in open channels as a function of the stream slope S, the mean flow depth H, and the median grain diameter d_{50} that describes channel roughness, so following a Manning-Strickler approach (Julien, 2010),

$$U = 5\left({}^{h}/{}_{d_{50}}\right)^{1/6}(gHS)^{1/2} \tag{7}$$

where $(ghS)^{1/2}$ represents the shear velocity u^{*}.

This calculated flow velocity U is compared at each cell location on the transport route with the deposition threshold velocity U_{depos}. If $U > U_{depos}$, the flow is moved into the destination cell and this calculation process is repeated.

Deposition of Sediment from Dispersive, Decelerating Flows

Deposition from a dispersive flow is proportional to the flow volume that passes into a cell. Deposition occurs where flow velocity, controlled by topographic slope, drops below a specified threshold velocity, so deposition commences in the first cell where flow velocity into the lowest adjacent cell is equal to or below the sediment deposition threshold U_{depos}. Until this point is reached, the flow is assumed to be strongly directional, flowing preferentially down the steepest gradient, or topographically constrained, for example in a channel or a canyon, feeding into the apex of the fan system. From this point down-dip, sediment transport becomes unconstrained and dispersive, with a progressively widening flow front, bathymetry permitting, and progressive deposition of sediment, to generate a typically lobate deposit. Starting from the cell occupied by the whole flow volume, flow volume moving into each surrounding cell is determined by the topographic gradient into that neighboring cell, following the general assumption that flow concentrates toward the direction of maximum slope. The proportion, ΔV_k, of sediment volume $V_{i,j}$ received by each surrounding cell is dependent on the gradient from the source cell G_k, so

$$\Delta V_k = \left[{G_k}^{FRF} \cdot \left(\sum_{k=1}^{8} G_k \right)^{-1} \right] \cdot V_{i,j} \qquad where \quad k = 1,2,3,\ldots,8; \tag{8}$$

modified from Trauth (2007), where the flow radiation factor FRF controls the degree of flow dispersion. Low values of FRF (≤ 1.0) lead to relatively high flow dispersion of the flow, generating a wider flow front and consequently wider lobes. Conversely, higher values of FRF (> 1.0) concentrate flow down the steepest slope, generating narrower, more elongate lobes.

For simplicity here, we assume that the dispersive flow doesn't have the velocity required to overcome topographic obstacles, so cells with higher elevation than a source cell receive no flow from that cell ($\Delta V_k = 0$). We also assume that cells that have already received deposition in a previous iteration of the flow front calculation will not receive any subsequent flow; such cells are not a valid flow destination during later iterations for the flow-front calculation. This is a necessary simplification to avoid long or possibly infinite computation time arising from looping flow patterns.

Sediment thickness deposited, $\Delta h_{i,j}$, during dispersive flow is calculated as a proportion of the sediment volume $V_{i,j}$ that flowed into the cell, so

$$\Delta h_{i,j} = {V_{i,j}\left(r_{depos} + DTF_t\right)} \Big/ {\Delta s^2} \qquad (9)$$

where r_{depos} is the fraction of the total sediment volume to be deposited in each cell, set as a basic input parameter in the model. For simplicity r_{depos} is kept constant through both model runs. During dispersive deposition, the deposit thickness factor (DTF) controls how deposition occurs, as a function of time through the flow transport, affecting the final lobe thickness and length. DTF > 0 will progressively increase the fraction of volume deposited at each new flow location. Conversely, when DTF < 0, r_{depos} will decrease while the flow is spreading. After deposition in newly occupied grid cells, any remaining sediment volume will carry on to the next down slope adjacent cells. If dispersive flow reaches a local basin with no lower adjacent cells, either the flow stops, or if there is sufficient flow volume, sufficient thickness is deposited to fill the local basin to the height of the lowest adjacent cell, and the flow can then continue into that same height cell and any lower surrounding cells as usual. Flow from any cell in the flow front ends when sediment volume in the cell falls below a defined minimum; in that case all the remaining sediment is deposited in the cell. Typical input parameter values, together with a brief explanation and rationale of each, are listed in Table 1.

Numerical Model Scenarios, Initial Conditions, and Parameter Values

Two Lobyte3D scenarios presented here represent a submarine-fan system modelled on a grid of 200 by 200 square cells each 100 m by 100 m. The same initial bathymetry, with a 5-km-long 1.15° slope margin and a flat basin floor (Figure 1A), is used in both cases. Both scenarios model 1000 flow events, interrupting background hemipelagic deposition occurring at rate 0.05 m ky^{-1} (Garrison, 1990). With a flow repeat time of 1000 years, maintained through each model run, each model scenario represents a plausible but simple representation of 1 My of flow history and deposition. The constant supply scenario has sediment volume of 2.0×10^5 m^3 per flow. The variable-supply scenario varies supply sinusoidally, with a period of 25 flows or 25 ky, a peak-to-peak amplitude of $3.0 \times 10^5 m^3$, and mean supply volume of $2.0 \times 10^5 m^3$. Both scenarios represent relatively small river systems, for example less than half the sediment supply rate of the Rhone river, producing a submarine fan comparable in size to small submarine fans on the California borderlands margin (Covault et al., 2007) and comparable in size to many outcrop and subsurface examples (e.g. Prelat et al., 2010; Sømme et al., 2011)**.** Initiation of the flows at the top of the slope is analogous to hyperpycnal flow sediment input directly from a shelf-edge delta river mouth, or more complex flow origins down a submarine-canyon.

All strata produced in each model scenario is saved as an output file to be statistically analyzed and plotted as cross sections (Figure 2A,B, D, E), vertical sections, and chronostratigraphic diagrams (Figure 2C and 2F). Stratigraphic completeness is calculated at each grid cell location as the proportion of total model layers that preserved some deposition from a flow (Fig. 3A and C). Meaningful identification of ordered strata requires use of quantitative evidence, so we analyze strata from the two model scenarios using two different methods. A bed-by-bed and laminae-by-laminae runs analysis identifies thinning- or thickening-upwards trends, and a spectral analysis that identifies any dominant frequencies in bed and laminae thicknesses using power-spectra analysis. Importantly, both methods are simple to carry out on vertical successions of outcrop strata, making these analyses also applicable to interpretation of deep-water-fan strata in outcrop or core.

Runs tests (Davies, 2002; Burgess, 2016) identify layer thickness trends looking for thinning-and thickening-upward patterns that could indicate presence of the periodic external signal (Fig. 2F). A runs test statistic *r* value that essentially counts consecutive beds that thin or thicken upwards, to form a trend or run, is calculated for each vertical section from the model. This *r* value is then compared against the range of equivalent *r* values calculated from randomly shuffled versions of the same strata generated using a 5000 iteration Monte Carlo approach. A *p* value is calculated for each section which indicates the probability that the modelled vertical succession of bed thicknesses could occur as a chance arrangement. Values of *p* less than 0.01 indicate a very low chance of the observed strata occurring by chance, and this is evidence of organized bed thicknesses within a vertical succession linked to either allocyclic forcing or autocyclic processes. Note that we consider only flow deposits with a thickness of 1 mm or greater, because anything thinner is unlikely to ever be practically measurable from outcrop analysis.

Spectral analysis involved computing the power spectrum from the observed vertical succession using the method from Menke and Menke (2016), and compares this spectrum with the spectra calculated from randomly shuffled versions of the same bed thicknesses using a similar 5000 iteration Monte Carlo approach. P values calculated for each frequency in the power spectra indicate if the amplitude is significant or is likely to occur just by chance. Peaks with significant power at the frequency of the external supply forcing would indicate preservation of the forcing signal in the strata, and significant peaks at other frequencies are likely to be either modifications of this signal by transport and depositional processes, or entirely autogenic in origin.

Results

Fan Stacking Patterns, Avulsions and Lobe Distribution

Both the constant-sediment-supply model scenario and the oscillating-supply model scenario generate a multi-km-scale submarine fan consisting of interbedded event beds and background hemipelagic strata (Fig. 1A, 2). Event-bed strata stack as lensoid or tapering packages exhibiting a typical width-to-thickness ratio of 300:1 in both strike and dip directions, and divided by laterally continuous layers of hemipelagic strata (Figure 2A,B,D, E). Gradients on depositional surfaces generally range from 0.5 degrees to flat, with a few cases of local gradients up to 0.8 degrees where thicker units are deposits in the updip sections of the fan. In both directions, individual beds onlap and/or downlap adjacent or underlying hemipelagic strata (e.g. Fig 2A, B). In both model scenarios, once initial fan topography has been constructed by the first 50 to 100 flows, strata begin to form qualitatively identifiable packages, each constructed from 5 to 60 contiguous spatially clustered flow events separated by lateral shifts in the focus of deposition (Fig. 2C, F) and periods of only hemipelagic deposition (Fig. 2). Within the packages unit thickness ranges from millimeter-scale laminae to beds up to over a meter thick (Fig. 2C, F, Table 2). Each vertical section from the model exhibits an approximately exponential thickness-frequency distribution, so there are many more thin units than thick units recorded, leading to a mean value for bed thickness in a vertical section that is much lower than the maximum bed thickness (Table 2). Some packages contain vertical thickness trends, measurable as runs of increasing or decreasing thickness, up to six units in length (Fig. 2C, F). Without quantitative evidence, such apparent trends are not evidence of order and, importantly, these qualitative properties of the modelled strata appear similar for both the constant-supply and the oscillating-supply scenarios. Overall, modelled strata from both scenarios are comparable to typical submarine-fan bathymetry and successions (Romans et al. 2009; Romans et al., 2010; Prélat and Hodgson, 2013) in terms of surface gradients and ranges and distributions of bed thicknesses and stacking patterns, suggesting that Lobyte3D is able to replicate fan strata in a simple but generally realistic manner.

The apparent organization of the strata into qualitatively identifiable packages containing apparent vertical thickness trends occurs due to repeated, rapid shifts in the locus of deposition, analogous to lobe-switching avulsion events that occur on many fan types in the natural world (see animations in data archive entry). Accumulating flows tend to convert bathymetry in the area of deposition from a concave-up low to a convex-up high as sediment accumulates. At some point, usually after between 5 and 60 flows, this ongoing aggradational and retrogradational stacking of strata (e.g., Fig. 2A, B) leads to a new steeper route across the fan. This steeper route is then exploited by the next series of depositional flow events, to deposit flows in a location some distance from the previous deposition (see sudden jumps in flow location through time, shown by sudden increases on the flow separation distance time series, Fig. 2C, F), and over time produce a new depositional lobe. This lobe-switching avulsion process occurs repeatedly but irregularly through time in both model runs (see animation in data archive entry), as a consequence of the feedback between flow routing and the evolving depositional topography. This is an emergent autogenic behavior. Strata observed in outcrop and the subsurface formed by this process are commonly referred to as compensationally stacked (e.g., Straub et al., 2009; Hajek et al., 2012), and may also be what outcrop studies often refer to as hierarchical (Prélat and Hodgson. 2013). Similar behavior has been observed in other recent forward modelling studies (Groenenberg et al., 2010; Harris et al., 2016). Observation of autogenic avulsion packages in the model raises two interesting questions that we can address here: does the autogenic avulsion behavior produce truly ordered strata identifiable with robust quantitative evidence, and does the lobe-switching process allow or inhibit recording of any external sediment-supply signal identifiable from analysis of vertical sections?

Identification of Order in 1D Vertical Sections

Runs-test p values, calculated from vertical sections across the fan strata modelled with no external sediment-supply signal, shows significant order ($p < 0.01$) over 23% of the fan area (Fig. 3B). Much of this order occurs in the mid fan (Fig. 3B). Stratigraphic completeness ranges from near zero across large areas of the distal and proximal fan, to around 54% stratigraphic completeness in the mid fan (Fig. 3A). Low p values, indicating stratal order, tend to occur in areas with higher stratigraphic completeness (y distances of 5 to 7 km, Fig. 3). This order may be detectable from outcrop analysis, at least from the thicker beds in each vertical section, which range up to 1.6 m, with mean values from 3 mm to 2 cm (Table 2). Low p values on the outer fan, where stratigraphic completeness is low, occur in strata where event beds have a mean thickness of only 1 mm or less (Table 2), so it is doubtful that this order would be identifiable from outcrop strata, and certainly not based on simple field observations and measurements. Since no periodic forcing is present in the constant-supply scenario, low p values indicating ordered strata must be arising in this case exclusively from autogenic bed-thickness trends produced by lobe-switching processes. This answers the first question raised above; in this model, autogenic processes generate ordered strata, highlighting the possibility that similar bed-thickness order observed in outcrop analysis could also be autogenic.

Runs-test p values calculated from modelled fan strata with periodically varying sediment supply show significant order ($p < 0.01$) over 26% of the fan area (Fig. 3D). Similar to the constant sediment supply scenario, much of this order occurs in the mid fan, where stratigraphic completeness reaches 65% and bed thickness is up to 1.57 m. So again, the best chance for outcrop detection of low p values is from areas with relatively high stratigraphic completeness in the more proximal and middle parts of the fan (dip distance y = 5-7 km, Fig. 3C, D). Comparing with the constant-supply scenario, in this periodic-signal scenario there is a slightly greater area of ordered strata, and a higher stratigraphic completeness (Fig. 3C). However, it is difficult to see how either the qualitative or quantitative evidence would permit a robust distinction between patterns of strata arising from allogenic forcing and patterns of strata arising from autogenic processes in this scenario.

Spectral analysis of the strata from both scenarios, with Monte Carlo testing of statistical signifance, builds on the runs analysis by identifying the frequency content in any bed-thickness trends, which can then be compared with an external signal frequency. For both constant and variable sediment-supply scenarios, few significant peaks occur in proximal fan positions (Fig. 4A,D), but in both mid and more distal fan settings from 5-8 km in the dip (y) direction, for both constant-supply and variable supply cases, there are many peaks with low p values that are unlikely to occur just by chance and so can be considered significant (Fig. 4B, C, E, F). In the constant supply model there are ≈29400 significant peaks across the fan strata (Fig. 5A, C, and see examples in Fig. 4B, C). Of these, a subset of 54 locations, representing ≈0.5% of the fan area, record a signal at the input frequency from the variable-supply model (Fig. 5A). Because there is no external signal in this constant-supply model run, these are peaks produced by autogenic processes that just happen to have the same frequency as the external signal.

In the variable-supply model there are ≈26100 significant peaks across the fan strata, of which 455, or ≈4.3% of the fan area, occur at the 1/layers = 0.04 25 ky input-signal frequency (Fig 5B, D, and see examples in Fig. 4E, F). These sections that record the external signal occur mostly in axial locations in the mid fan area, from y = 5.9 km to 6.9 km, with outlier points from 7.5 km to 8.2 km in the constant supply scenario (Fig. 5A), and from y = 5.3 km to 8.5 km in the oscillating-supply scenario (Fig. 5B). Stratigraphic completeness is highest in this part of both fans (Fig. 3A, B, D, E) and most of the packages of strata produced by lobe-switching avulsion events have layers that extend into at least part of this area, especially when lamination-scale strata that make up the large majority of the beds (Table 2) are considered (e.g., see the strike cross section for the variable-supply scenario, Fig. 2E, from 10 to 12 km).

The total number of spectral peaks at each frequency (Fig. 5C, D) summarizes the difference in signal content recorded in the strata from the two model scenarios. While the constant-supply model shows an approximately exponential decline in number of significant peaks with increasing frequency (Fig. 5C), suggesting no characteristic scale for autogenic cyclicity, the same decreasing trend in the variable-supply-scenario is interrupted by an increase in number of significant peaks around the frequency of the input signal; there are ≈2500 extra significant peaks in the variable-supply-scenario power spectra between frequency 0.05 and 0.03, forming what we refer to as a “signal bump” on the distribution (Fig. 5D). The “signal bump” frequency range corresponds to cycles of between 20 and 33 layers, suggesting that the input signal (25 layers per cycle) is being modified in a rather complex way, and as already stated may not be easily recognizable in individual vertical sections, especially when autocycles are also present. Based on these model examples, in order to distinguish with reasonable certainty significant peak frequency counts arising from allogenic forcing (Fig. 5D) versus an autogenic equivalent (Fig. 5C), it will be necessary to measure and analyze enough vertical sections to distinguish a frequency distribution of significant peaks with the autogenic form (Fig. 5C) versus a distribution with the allogenic form (Fig. 5D). Further testing is required to determine how many vertical sections would need to be measured to accurately determine which shape of distribution is present but, for example, one hundred logged sections would certainly give a more robust answer than just ten, so outcrop data collection may have to increase by an order of magnitude. These model results also indicate that the most efficient place to do this data collection would be the mid-fan axial zone, where stratigraphic completeness and external signal expression is highest in the variable-supply model scenario (the green area in Figure 5B); if the "signal bump" is not expressed in strata in this area, it is perhaps unlikely to be present.

In summary, power-spectrum analysis and runs tests on strata from the two model scenarios shows that even in the externally forced model, allogenic stratal order may not be straightforward to identify without good information about the input signal and how it influences strata, because while an external signal can potentially be preserved, autogenic processes can also create significant, detectable order in the form of statistically significant thickening and thinning trends in the strata (e.g., Fig. 3B). Even when an element of the external signal is present, it is often only partly preserved remnants of the same signal (Fig. 4E, F), and degree of preservation varies across the fan surface (Fig 4, compare all six example locations, and Fig 5B). This suggests an answer to the second question posed above; shifting location of deposition, analogous to avulsion and lobe switching, complicates recording of a strong external sediment supply signal across the whole fan, but some signal may still be detectable. It is likely that any signal present will be broken down into higher-frequency remnants, or merged into lower-frequency apparent signals, that will likely be difficult to robustly identify as an external signal, especially given the presence of similar autogenic patterns. The results suggest a hypothesis that quantitative analysis of many densely spaced 1D vertical sections or 2D cross sections through the mid-fan axial zone may be an effective way to search for preservation of an external signal by constructing a significant peak frequency count.

Discussion

These Lobyte3D model results support outcrop interpretations that suggest that lobe development and compensational stacking are guided principally by basin-floor topography at a variety of scales (Hodgson et al., 2006; Prélat et al., 2013; Straub and Pyles, 2012; Spychala et al., 2017) independent of extrinsic controls. However, although lobe formation and compensational stacking of beds is a deterministic process, the history of previous deposition imparts complex pattern to the strata, including entirely autogenic elements of onlap, downlap, progradation, and retrogradation (Fig. 2A,B, D, E), such that allocyclic pattern and signal may be difficult to distinguish visually or even quantitatively from autocyclic trends and patterns. Routing of flows over a complex seafloor topography produced by earlier flows also tends to break up the external signal, due to low stratigraphic completeness in each location. This is not quite the same as the signal shredding process, defined by Paola (2017) as “sediment storage–release processes, acting over a wide range of scales,” that “take a periodic input signal and disperse (‘‘shred’’) it over the autogenic scale range such that at the downstream end of the system the signal is not merely obscured but rather destroyed”. However, it is a related process; what happens in Lobyte3D is analogous to one step in the shredding process, which if repeated would certainly destroy any input signal. For example, if a similar flow-routing process occurred farther up the sediment-routing systems, with subsequent erosion, transport, and redeposition, signal shredding would likely ensue.

Analysis and comparison of strata from the two model scenarios suggests that reliable identification of an external signal, either visual identification, identification with simple statistics, or even identification using spectral analysis of a 1D vertical section, would be possible only with substantial *a priori* information about the likely depositional response to both allogenic and autogenic processes, for example the number of flow events or layers likely to occur in each allocyclic supply oscillation. This is unlikely to be information we would have or be able to reliably determine for any outcrop or subsurface example. Also, even in cases with good independent information on the signal period, and how it relates to bed and lobe-scale depositional events, signal detection may be difficult with only limited 1D or 2D data because autogenic processes produce similar trends and frequencies of variation in the quantitative analyses. Based on this we might conclude that the optimum situation set for a stratigrapher to be able to recognize an unambiguous sediment-supply signal in lobate fan strata will likely be a 3D dataset with high-resolution dating that allows volume measurements to reconstruct flow history and hence supply history (e.g., Sømme et al., 2011).

However, analysis of the count of significant peaks that occur across the range of frequencies in a power spectrum (Figure 5C, D) may facilitate detection from 1D or 2D stratigraphic data. The distinction between an approximately exponential decrease of the count of significant peaks with frequency in an autogenic systems (Fig. 5C) and the “signal bump” in the count distribution arising from the combined autogenic and allogenic model (Fig. 5D) could allow identification of a signal from information on layer thickness in an outcrop or subsurface example, without *a priori* assumptions or information about how the signal affects deposition in the system. Testing for presence of the “signal bump” in the kind of deep-water fan system modelled here may seem like a substantial task, requiring recording and analysis of a substantial number of vertical sections, or crosssection. However, data of this type and density are increasingly common.

These model results suggest that the axial mid-fan zone is the area most likely to contain identifiable signal. This may simply be because the axial mid-fan zone is the best candidate for spatial overlap of successive system-wide lobe, but the exact reasons for this require more investigation. We hypothesize that it is likely related to the ratio between key autogenic timescales and the allogenic timescale (t_s). Consider two autogenic processes that operate at different spatial scales and time scales: lobe switching and flow switching. Lobe switching occurs at a larger system-wide scale and at a timescale t_l, and flow switching occurs at a smaller, lobe-wide scale. Both processes are determined by topographic-flow(s) feedback and lead to compensational stacking, at different temporal and spatial scales. The flow-switching autogenic process is driven by the interaction of topography and individual flow events, on an event-by-event basis, and the deposition of individual beds. This flow-switching process and compensational stacking directly influences *at-a-point* bed thickness over time (Straub and Pyles, 2012), in the absence of allogenic forcing. Given that we are interested in the capacity of 1D vertical bed thickness trends to record allogenic sediment-supply signals, we must first ensure that we define a thickness of strata within a 1D vertical section that contains the full autogenic distribution of bed thickness, i.e., a compensational stack of beds. The timescale required for the generation of a compensational stack of beds is t_{cp}. A first-pass estimate of whether a given periodic allogenic sediment supply (t_s) can be identified from within a cluster of 1D vertical sections should consider timescales t_l and t_{cp}, even if the consideration is arbitrary. For example the likelihood that a cluster of sections in a particular region will contain evidence of allogenic signals will be greater if $t_l >> t_{cp}$ and $t_l >> t_s$. So low-frequency sediment-supply signals can be shredded by lobe switching autogenics at the larger scale (i.e.

ts < tl), and high-frequency sediment-supply signals are potentially shredded by flow-routing autogenics at the smaller scale (i.e., $t_s < t_{cp}$). An appropriate way to approximate these autogenic timescales in the field is needed (e.g., Ganti et al., 2016), and this hypothesis requires further testing, first with analogue and numerical experiments of submarine fans, and then again against outcrop and subsurface data examples (e.g., Straub and Pyles, 2012; Li et al. 2016).

A long history of sequence stratigraphic studies, influenced by the sequence stratigraphic model that emphasizes allogenic forcing, have proposed that sand-prone submarine lobe strata are separated by regional hemipelagic mudstones that mark highstand and transgressive shutdown in coarse supply to the deep basin (e.g., Flint et al. 2011). However, Spychala et al. (2017) interpret several genetically related lobe complexes, separated by hemipelagic strata, as part of the same lowstand systems tract. In outcrop, fine-grained, thin-bedded interlobe units can be interpreted to represent allogenic reduction in sediment supply (Johnson et al., 2001; Hodgson et al., 2006) or autogenic switching of lobes (Prelat et al., 2009). A stratigraphic criterion for distinguishing between an allogenic and autogenic interpretation requires tracing units laterally and up dip, to establish if these interlobe units are autogenic and pass laterally into lobe strata, or if they are laterally extensive and therefore likely allogenic (Spychala et al., 2017). These Lobyte3D results demonstrate that laterally persistent interlobe units can extend across a ”lobe complex” and indeed across most of the fan surface (Figure 2A, B, D, E) even when the system is entirely autogenic, simply as a consequence of how normal background sedimentation processes interact with localized flow deposition.

In summary, these Lobyte3D numerical-modelling results suggest that fan strata may be more complex than often considered, due to the important influence of autogenic processes, making identification of an external signal difficult but not impossible, even from limited 1D vertical section data. Further investigation of depositional processes, even with reduced complexity models like Lobyte3D, combined with consideration of the type and resolution of data collected from outcrop and subsurface studies, is increasingly necessary (Straub and Pyles, 2009; Foreman and Straub, 2017), as well as a careful evaluation of how we interpret and apply such data. Specifically, in the next steps in this research we will use Lobyte3D to explore how a range of signal frequencies and amplitudes are preserved or obscured in fan strata using the signal-bump method, and hopefully those results will then prove useful for outcrop and subsurface interpretation. More generally, this study demonstrates that perhaps it is time to move away from model-driven interpretations that simply assume simply expressed external signals? Maybe it would be more useful instead to generate new, testable hypotheses about the nature of strata from numerical and analogue forward models, and let 2D and 3D high-resolution outcrop and subsurface data speak more independently to test those hypotheses?

Conclusions

1. Lobyte 3D is a reduced-complexity model of deposition in dispersive-flow fan systems the shows emergent behavior such as lobe switching and compensational stacking of a potentially hierarchical nature due to flow over a complex, evolving seafloor topography.
2. Strata from two Lobyte3D scenarios, one with constant sediment input, and one with oscillating sediment input, show clustering of beds and, in places, ordered strata even without any allogenic signal. Ordered, autocyclic variations in bed thickness arise due to deposition repeatedly shifting on the fan surface and revisiting previous locations of deposition, but despite the order, this process is variable and complex, and in these results has little or no characteristic frequency.

3. An allogenic signal is present in places in the oscillating-supply scenario, but it would be difficult to distinguish from the autocyclic elements without knowing *a priori* how the signal frequency is likely to be recorded in the strata.
4. These initial modelling results suggest that a useful approach to identify an external from outcropping fan strata is to measure many 1D vertical sections in the axial area of the mid fan, where stratigraphic completeness is high and many flows are likely to be recorded. Analysis of the sections using simple power-spectrum methods and counting of the significant peaks present across a range of frequencies may allow identification of a "signal bump" that could be evidence of the presence and nature of allocyclic forcing. Further work is required to test this further and determine if and how the "signal bump" is preserved with input signals across a range of frequencies and amplitudes.
5. Even a reduced-complexity numerical stratigraphic forward model like Lobyte3D produces stratigraphic behavior more complex than many stratigraphic conceptual models and interpretations account for. Almost certainly real depositional systems are even more complex. This deficit in the complexity of our stratigraphic interpretations and analysis methods needs to be addressed, perhaps by more integration of outcrop and experimental modelling analysis.

Acknowledgments

Masiero would like to acknowledge financial support from Tullow Oil, Woodside Petroleum, and Wintershall. Toby would like to thank Silvio De Angelis for guidance in the power-spectra analysis. Zoltan Sylvester, an anonymous reviewer, and associate editor Kyle Straub provided many constructivecomments on the original manuscript that were very useful helping us better explain and

focus our arguments. Lobyte3D source code and animations from the two model cases in this paper are available in the JSR data archive at https://www.sepm.org/JSR-Data-Archive.

References

Anderton, R., 1995, Sequences, cycles and other nonsense: are submarine fan models any use in reservoir geology?, in Hartley, A.J., and Prosser, D.J., (eds.), Characterzation of deep-marine clastic systems, Geological Society of London, Special Publication , p. 5-11, https://doi.org/10.1144/GSL.SP.1995.094.01.02

Bokulich, A., 2013, Explanatory Models Versus Predictive Models: Reduced Complexity Modeling in Geomorphology, in: Karakostas, V., and Dieks, D. (eds.), EPSA11 Perspectives and Foundational Problems in Philosophy of Science; The European Philosophy of Science Association Proceedings 2, p. 115-128. DOI 10.1007/978-3-319-01306-0.

Burgess, P.M., 2006, The Signal and the Noise: Forward Modeling of Allocyclic and Autocyclic Processes Influencing Peritidal Carbonate Stacking Patterns, Journal of Sedimentary Research, v. 76, p. 962-977.

Burgess, P.M., 2013, CarboCAT: A cellular automata model of heterogeneous carbonate strata, Computers and Geoscience, v. 53, p. 129-140.

Burgess, P.M., 2016, Identifying ordered strata: Evidence, methods, and meaning; Journal of Sedimentary Research, v. 86, p. 148-167.

Covault, J.A, Normark, W.R., Romans, B.W, and Graham, S.A., 2007, Highstand fans in the California borderland: The overlooked deep-water depositional systems: Geology, v. 35, p.783-786.

Davis, J.C., 2002, Statistics and Data Analysis in Geology: New York, John Wiley and Sons, 638 p.

Flint, S.S., Hodgson, D.M., Sprague, A.R., Brunt, R.L., Van der Merwe, W.C., Figueiredo, J., Prélat, A., Box, D., Di Celma, C., and Kavanagh, J.P., 2011, Depositional architecture and sequence stratigraphy of the Karoo basin floor to shelf edge succession, Laingsburg depocentre, South Africa: Marine and Petroleum Geology, v. 28, p. 658-674.

Gong, C., Blum, M.D., Wang, Y., Lin, C. and Xu, Q., 2018, Can climatic signals be discerned in a deep-water sink?: An answer from the Pearl River source-to-sink sediment-routing system: Geological Society of America Bulletin, v. 130, p. 661–677. https:// doi .org /10 .1130 /B31578 .1

Foreman, B.Z., and Straub, K.M., 2017, Autogenic geomorphic processes determine the resolution and fidelity of terrestrial paleoclimate records: Science Advances, v. 3, no. 9, e1700683, doi: 10.1126/sciadv.1700683.

Ganti, V., Chadwick, A.J., Hassenruck Gudipati, H.J., and Lamb, M.P., 2016, Avulsion cycles and their stratigraphic signature on an experimental backwater-controlled delta, Journal of Geophysical Researchc Earth Surface, v. 121, p. 1651-1675, doi:10.1002/ 2016JF003915.

Garrison, R.E., 1990, Pelagic and hemipelagic sedimentary rocks as source and reservoir rock, in Brown, G.C., Gorsline, D.S., and Schweller, W.J., eds., Deep Marine Sedimentation Depositional Models and Case Histories in Hydrocarbon Exploration and Development: Pacific Section SEPM., v. 66, p.123-149.

Groenenberg, R.M., Hodgson, D.M., Prelat, A., Luthi, S.M., and Flint, S.S., 2010, Flow-deposit interaction in submarine lobes: Insights from outcrop observations and realizations of a process-based numerical model: Journal of Sedimentary Research, v. 80, p. 252–267, doi: 10.2110/jsr.2010.028.

Hajek, E.A., Heller, P.L., and Schur, E.L., 2012, Field test of autogenic control on alluvial stratigraphy (Ferris Formation, Upper CretaceousPaleogene, Wyoming): Geological Society of America, Bulletin, v. 124, p. 1898–1912, doi: 10.1130/B30526.1.

Harris, A.D, Covault, J.A., Madof, A.S., Sun, T., Sylvester, Z., and Granjeon, D., 2016, Three-dimensional numerical modeling of eustatic control on continental margin sand distribution: Journal of Sedimentary Research, v. 86, p. 1434-1443, doi: http://dx.doi.org/10.2110/jsr.2016.85.

Hawie, N., Covault, J.A., Dunlap, D., and Sylvester, Z., 2017, Slope-fan depositional architecture from high-resolution forward stratigraphic models: Marine and Petroleum Geology, v. 91, p. 576-585.

Hodgson, D.N., Flint, S.S., Hodgetts, D., Drinkwater, N.J., Johannessen, E.P., and Luthi, S.M., 2006, Stratigraphic evolution of fine-grained submarine fan systems, Tanqua Depocenter, Karoo Basin, South Africa: Journal of Sedimentary Research, v. 76, p. 20-40.

Johnson, S.D., Flint, S.S., Hinds, D., and Wickens, H.-de-V., 2001, Anatomy of basin floor to slope turbidite systems, Tanqua Karoo, South Africa: sedimentology, sequence stratigraphy and implications for subsurface prediction: Sedimentology, v. 48, p. 987-1023.

Julien, P., 2010, Erosion and Sedimentation: Cambridge, UK, Cambridge University Press, p.281 doi:10.1017/CBO9780511806049.

Kneller, B., and Buckee, C., 2000, The structure and fluid mechanics of turbidity currents: a review of somerecent studies and their geological implications: Sedimentology, v. 47, p. 62-94.

Knight, J., and Harrison, S., 2012, The impacts of climate change on terrestrial Earth surface systems: Nature Climate Change, v. 3, p. 24-29.

Li, Q., Yu, L., and Straub, K.M., 2016, Storage thresholds for relative sea-level signals in the stratigraphic record: Geology, v. 44, p. 1-4, doi: 10.1130/G37484.1.

Mayall, M., Jones, E. and Casey, M., 2006, Turbidite channel reservoirs - Key elements in facies prediction and effective development: Marine and Petroleum Geology, v. 23, p. 821-841.

Menke, W., and Menke, J., 2016, Environmental data analysis with Matlab: Cambridge, Massachusetts, Academic Press, 342 p.

Moore, I.D., Grayson, R.B., and Ladson, A.R., 1991, Digital terrain modelling: A review of hydrological, geomorphological and biological applications, Hydrological Processes, v. 5, p.3-30.

Mulder, T., Alexander, J., 2001. The physical character of subaqueous sedimentary density flow and their deposits. Sedimentology, v. 48, p. 269–299. doi:10.1046/j.1365-3091.2001.00360.x

Paola, C., 2017, A mind of their own: Recent advances in autogenic dynamics in rivers and deltas, *in* Budd, D.A., Hajek, E.A., and Purkis, S.J., eds., Autogenic Dynamics in Sedimentary Systems, SEPM, Special Publication106, p. 5-17. doi: 10.2110/sepmsp.106.04

Prélat, A., Covault, J.A., Hodgson, D.M., Fildani, A., and Flint, S.S., 2010, Intrinsic controls on the range of volumes, morphologies, and dimensions of submarine lobes: Sedimentary Geology, v. 232, p. 66–76, doi: 10.1016/j.sedgeo.2010.09.010.

Prélat, A., and Hodgson, D.M., 2013, The full range of turbidite bed thickness patterns in submarine lobes: controls and implications: Geological Society of London Journal, v. 170, p. 209–214, doi: 10.1144/jgs2012-056.

Prélat, A., and Hodgson, D.M., and Flint, S.S., 2009, Evolution, architecture and hierarchy of distributary deep-water deposits: a high-resolution outcrop investigation from the Permian Karoo Basin, South Africa: Sedimentology, v. 56, p. 2132-2154, doi: 10.1111/j.1365-3091.2009.01073.

Reitz, M.D., Jerolmack, D.J., and Swenson, J.B., 2010, Flooding and flow path selection on alluvial fans and deltas: Geophysical Research Letters, v. 37, L06401, doi:10.1029/2009GL041985.

Romans, B.W., Normark, W.R., McGann, M.M., Covault, J.A., and Graham, S.A., 2009, Coarse-grained sediment delivery and distribution in the Holocene Santa Monica Basin, California: Implications for evaluating source-to-sink flux at millennial time scales: Geological Society of America Bulletin, v. 121, p. 1394–1408. doi: 10.1130/B26393.1.

Romans, B.W., Fidani, A., Hubbard, S.M., Covault, J.A., Frostick, J.C., and Graham, S.A., 2010, Evolution of deep-water stratigraphic architecture, Magallanes Basin, Chile: Marine and Petroleum Geology, v. 28, p. 612-628.

Rothman, J.W., Simpson, J.E., Hunt, J.C.R., and Britter, R.E., 1985, Unsteady gravity current flows over obstacles: Some observations and analysis related to the phase II trials. Journal of Hazardous Materials, V.11, p. 325–340. Doi:10.1016/0304-3894(85)85044-5.

Sinclair, H.D., and Cowie, P.A., 2003, Basin-floor topography and the scaling of turbidites: The Journal of Geology, v. 111, p. 277–299, doi: 10.1086/373969.

Sømme et al., 2011, Linking onshore-offshore sediment dispersal in the Golo source-to-sink system (Corsica, France) during the late Quaternary, Journal of Sedimentary Research, v. 81, p. 118–137, doi: 10.2110/jsr.2011.11.

Spychala, Y.T., Hodgson, D.M., Prélat, A., Kane, I.A., Flint, S.S., and Mountney, N.P., 2017, Frontal and lateral submarine lobe fringes: Comparing sedimentary facies, architecture and flow processes: Journal of Sedimentary Research, v. 87, p. 75–96, doi: 10.2110/jsr.2017.2.

Straub, K.M., Paola, C., Mohrig, D., Wolinsky, M.A., and George, T., 2009, Compensational stacking of channelized sedimentary deposits: Journal of Sedimentary Research, v. 79, p. 673–688.

Straub, K.M., and Pyles, D.R., 2012, Quantifying the hierarchical organization of compensation in submarine fans using surface statistics: Journal of Sedimentary Research, v. 82, p. 889–898, doi: 10.2110/jsr.2012.73.

Talling, P.J., 2001, On the frequency distribution of turbidite thickness: Sedimentology, v. 48, p. 1297–1329, doi: 10.1046/j.1365-3091.2001.00423.x.

Talling, P.J., 2014, On the triggers, resulting flow types and frequencies of subaqueous sediment density flows in different settings: Marine Geology, v. 352, p. 155–182, doi: 10.1016/j.margeo.2014.02.006.

Teles, V., Beno�t Chauveau, Philippe Joseph, Pierre Weill, Fakher Maktouf, 2016, CATS – A process-based model for turbulent turbidite systems at the reservoir scale: Comptes Rendus Geoscience, v. 348, p. 489-498.

Thomopoulos, N.T., 2012, Essentials of Monte Carlo Simulation: Statistical methods for Building Simulation Models, New York, Springer Science & Business Media, 174 p., doi 10.1007/978-1-4614-6022-0

Trauth, M., 2007. MATLAB Recipes for Earth Sciences. doi.org/10.1007/978-3-540-72749-1

Wang, X., Luthi, S.M., Hodgson, D.M., Sokoutis, D., Willingshofer, E., and Groenenberg, R.M., 2017, Turbidite stacking patterns in salt-controlled minibasins: Insights from integrated analogue models and numerical fluid flow simulations: Sedimentology, v. 64, p. 530–552, doi: 10.1111/sed.12313.

FIGURE CAPTIONS

Figure 1. A) Model configuration showing the grid used in the two models presented here, and the total fan thickness deposited by 1000 flows in the scenario 2 model output. The two semitransparent rectangles show the location of the along-strike (Fig. 2B, E) and down-dip cross sections (Fig. 2A, D), and the arrow indicates the point of entry onto the grid for all the sediment flows. Note that a thickness cutoff in the plotting makes some thin but continuous strata on the edge of the fan appear discontinuous. B) A subset of the model grid showing sea floor topography towards the end of a Lobyte3D model run. The red line is the steepest-descent route a singleevent package of sediment would follow over the topography formed by previous fan lobes. The yellow squares show locations of deposited sediment from the flow, which became dispersive and depositional when the topographic gradient and hence flow velocity dropped below the threshold for sediment deposition.

Figure 2. A) Dip section through strata from the constant-supply model scenario along section line shown in Figure 1A. Event beds are color coded a shade between red and yellow to distinguish successive flow deposits, and hemipelagic strata are gray. Note clustering of flow-event deposition into discernible packages, separated by hemipelagic strata, and some complex patterns of bypass, basinward shifts in deposition, followed by retrogradational backstepping and onlap. B) Strike section through strata from the constant-supply model scenario along section line shown in Figure 1A. Clustering of flow-event deposition into discernible packages is also visible in this strike section. C) A vertical section from the constant-supply model scenario. The vertical section is located at the point where the lines of section in A and B intersect, shown as a vertical line in Figs. 2A, B, D, and E. The vertical section is correlated with time-equivalent positions in the strata plotted as a chronostratigraphic diagram. Adjacent to the chronostratigraphic diagram the number of runs up or down present in strata of each

age is shown, along with a time series showing the separation distance of successive flow-deposits centroids, and the external sediment supply history, all plotted on the same time axis. Squares marked on the flow centroid separation time series indicate the 20 largest flow offsets, analogous to avulsions events on the fan, often with corresponding on-off behavior on the chronostrat plot. See text for discussion D) Dip section through strata from the variable-supply model scenario along section line shown in Figure 1A. Note that the variations in bed thickness arising from variable supply are visible, especially some relatively thick units, but otherwise stacking of strata is not obviously different from the constant supply case shown in part A. E) Strike section through strata from the variable-supply model scenario along section line shown in Figure 1A, showing similar differences and similarities to the constant-supply case in Figure 1B. F) Vertical section and correlated chronostratigraphic diagram, number of runs, time series of flow centroid separation, and the history of external sediment supply, section position shown as a vertical line in Figs. 2A,B,D,& E. Note that, despite the external forcing, the number of runs appears similar to the constant-supply case in C.

Figure 3. A) Stratigraphic-completeness map for the constant-supply scenario, calculated as the proportion of total model time steps recorded by deposition from a flow. B) Runs- analysis *p* values for the constant supply scenario. Note there is a 1 cm total thickness cutoff off in the plotting, which creates the complex down-dip stratal termination, and shows that distal fan strata are very thin.See text for discussion. C) Stratigraphic-completeness map for the variable-supply scenario, calculated as the proportion of total model time steps recorded by deposition from a flow. D) Runs-analysis *p* values for the variable-supply scenario. Note the similar occurrence of *p* values less than 0.01 in both part B and part D, suggesting a similar level of ordered strata detected in both scenarios, despite the lack of external forcing in the constant-supply scenario.

Figure 4. Power spectra from a proximal (y 4 km), mid (y 5 km) and more distal (y 6 km) position on the axial zone of the fan (x 10 km) in each model scenario. Power spectra show peaks indicating dominant frequencies in the strata. In each case statistical significance of these peaks is calculated using a Monte Carlo approach (Thomopoulos, 2012; Burgess, 2016) that uses randomly shuffled and therefore mostly disordered, but otherwise equivalent, sections as a random model for comparison with the actual modelled section. Green dashed lines is the 99% confidence level calculated using this approach, and color coding shows *P* values each frequency, white being $P < 0.01$ therefore high significance. Vertical blue line marks the exact frequency of the external-supply signal with period 0.025 My. Curves show a mixture of no significant order (all peaks in yellow and red area, below green dashed line), and autogenic and allogenic signals. See text for discussion.

Figure 5. A) Map showing the distribution of points on the fan that show a significant signal at the frequency of the supply oscillations in the variable-supply scenario (green points). Red points represent spectra with largest peaks at frequencies lower than this variable-scenario input frequency, and violet represents spectra with largest peak at higher frequencies. In this constant-supply scenario, 0.48% of the fan area has spectra with peaks at this external signal frequency, all in a mid-fan setting, and concentrated mostly on or near the fan axis. B) Map showing distribution of spectra with significant signal frequency present, plus the distribution of highest power in the lower or higher frequencies, for the variable-supply model. In this case more of the fan area has peaks at the external signal frequency, again concentrated mostly in the axial zone of the mid fan, but still only 4.29% of the total fan area, so overall, the spatial distribution of spectral peak types is similar to the constant-supply case. C) The total number of significant (p<0.01) peaks at each frequency in the power spectra from all vertical sections on

the constant-supply-scenario fan. The vertical blue line indicates the frequency of the external supply signal in the variable-supply scenario. D) The total number of significant (p < 0.01) peaks at each frequency in the power spectra from all vertical sections the variable-supply-scenario fan. The vertical blue line indicates the frequency of the external-supply signal. Note the increased number of peaks around this frequency, referred to as a "signal bump", compared to the constant-supply case, which does not show this feature (C).

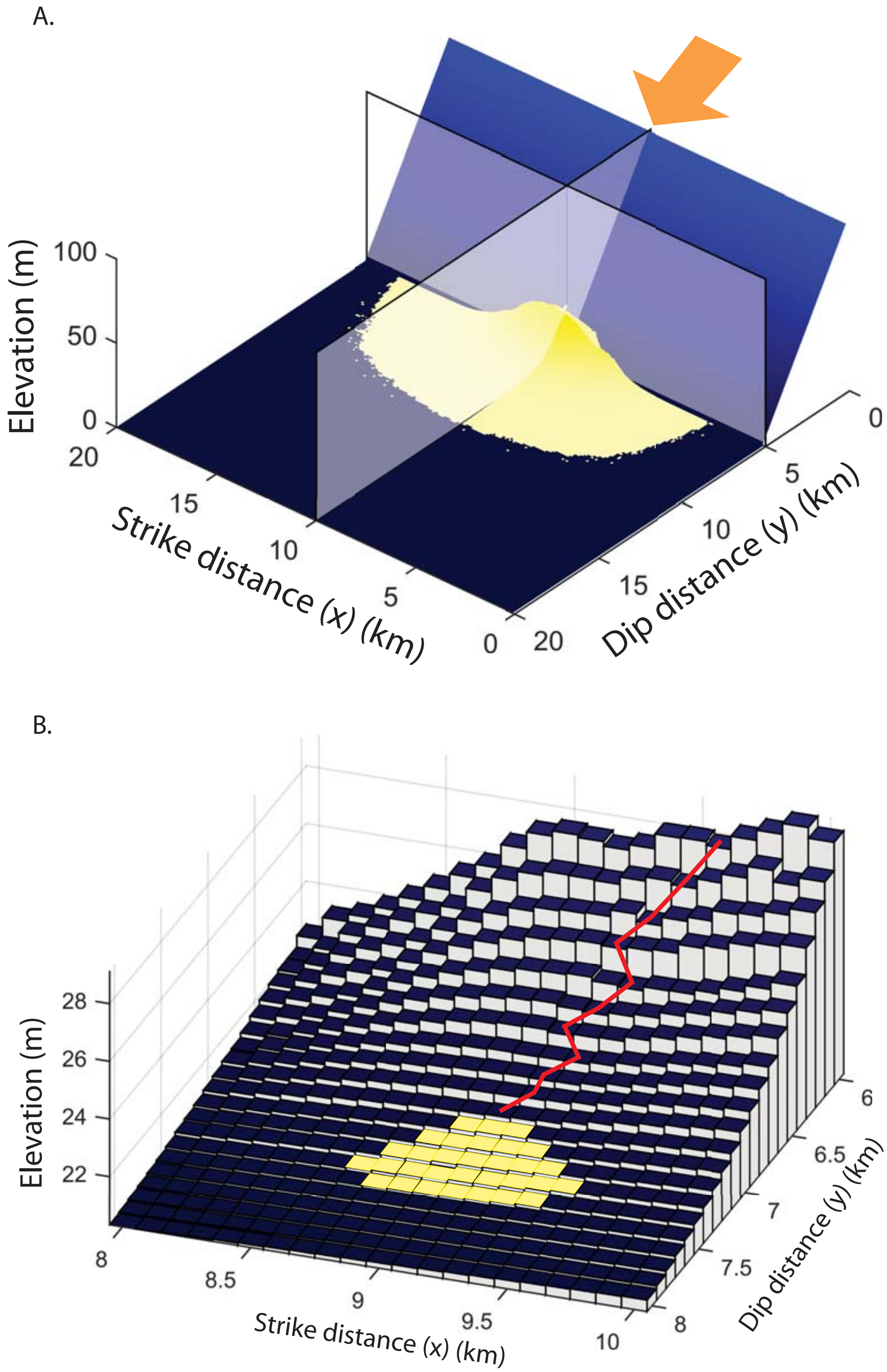

A.
Elevation (m)
100
50
0
20
15
10
5
0
Strike distance (x) (km)
0
5
10
15
20
Dip distance (y) (km)
B.
Elevation (m)
28
26
24
22
8
8.5
9
9.5
10
Strike distance (x) (km)
6
6.5
7
7.5
8
Dip distance (y) (km)

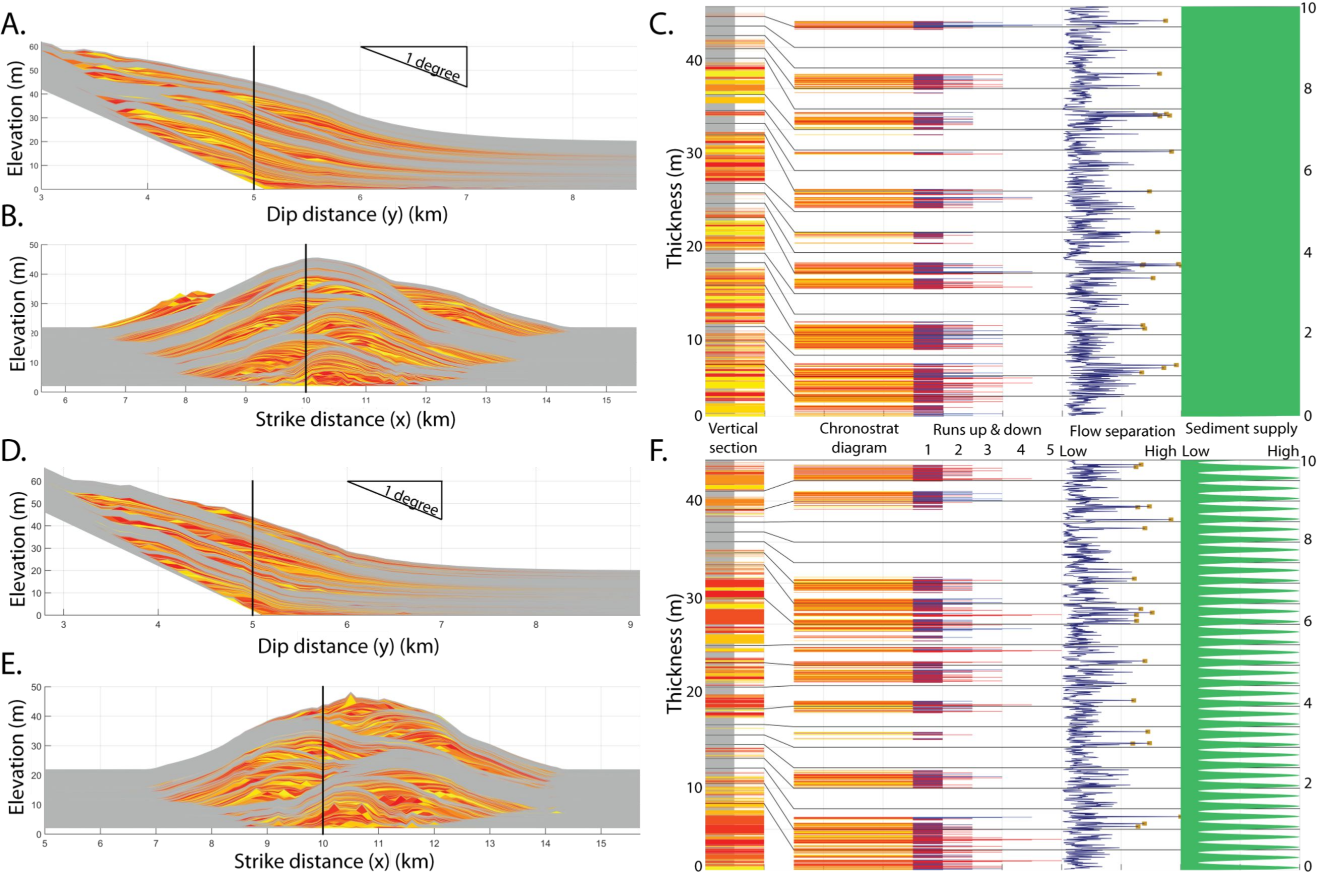

A.
Elevation (m)
1 degree
Dip distance (y) (km)
B.
Elevation (m)
Strike distance (x) (km)
C.
Thickness (m)
Elapsed model time (My)
Vertical section
Chronostrat diagram
Runs up & down
1 2 3 4 5
Flow separation
Low High
Sediment supply
Low High
D.
Elevation (m)
1 degree
Dip distance (y) (km)
E.
Elevation (m)
Strike distance (x) (km)
F.
Thickness (m)
Elapsed model time (My)

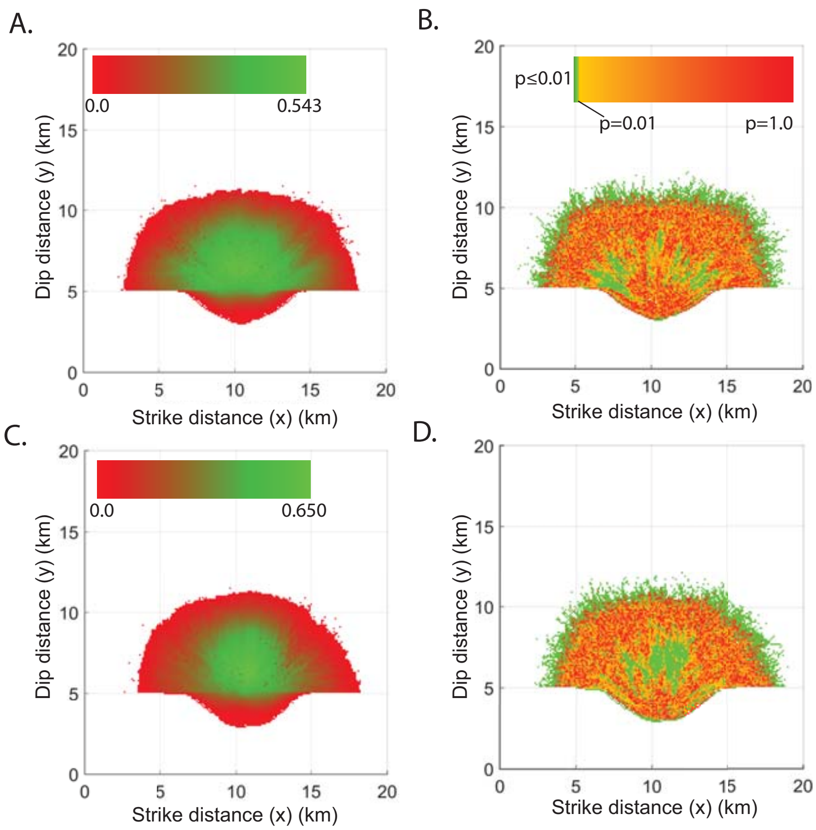
A.
0.0
0.543
Dip distance (y) (km)
Strike distance (x) (km)
B.
p≤0.01
p=0.01
p=1.0
Dip distance (y) (km)
Strike distance (x) (km)
C.
0.0
0.650
Dip distance (y) (km)
Strike distance (x) (km)
D.
Dip distance (y) (km)
Strike distance (x) (km)

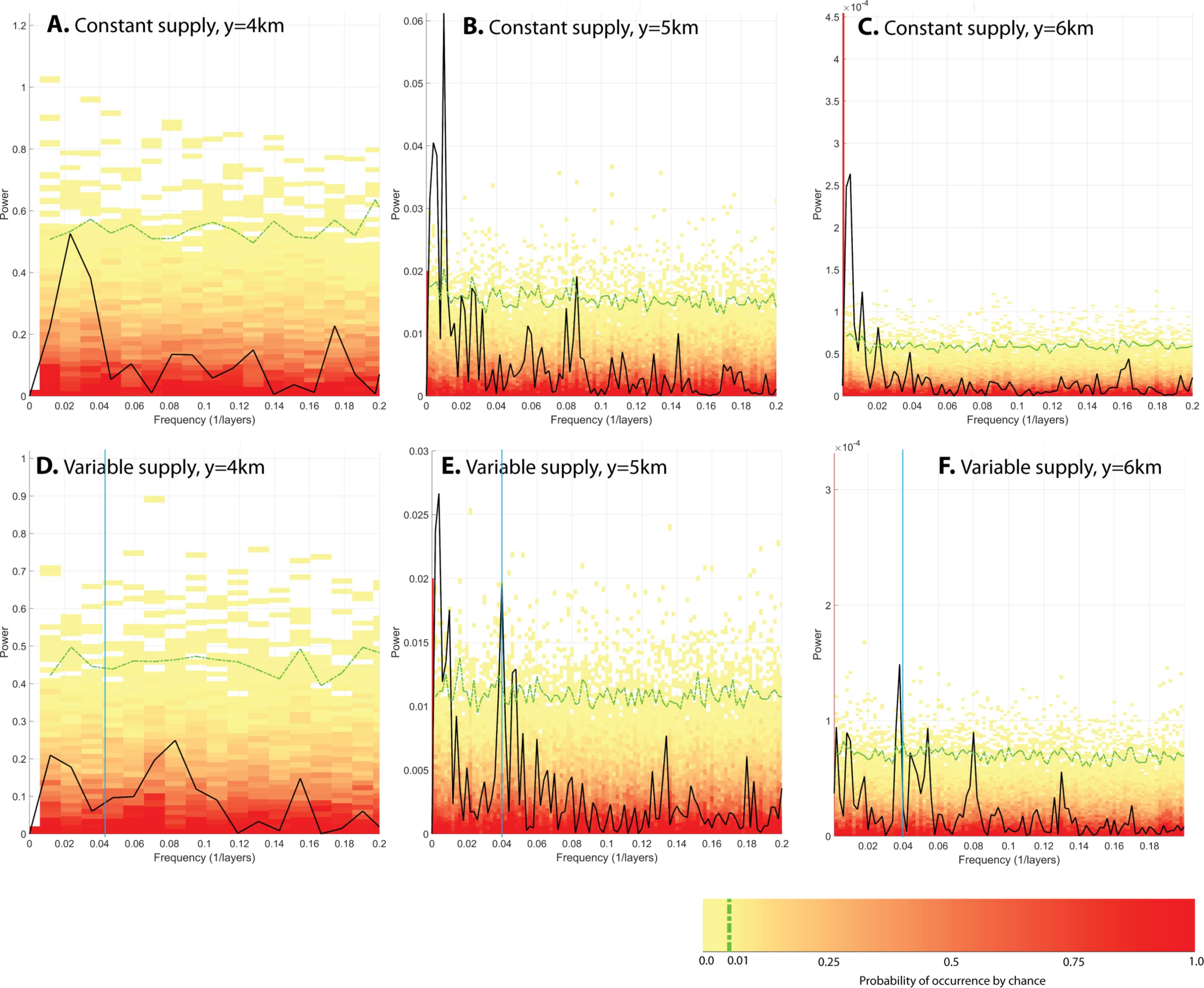
A. Constant supply, y=4km
B. Constant supply, y=5km
C. Constant supply, y=6km
D. Variable supply, y=4km
E. Variable supply, y=5km
F. Variable supply, y=6km
Power
Frequency (1/layers)
×10^-4
0.0
0.01
0.25
0.5
0.75
1.0
Probability of occurrence by chance

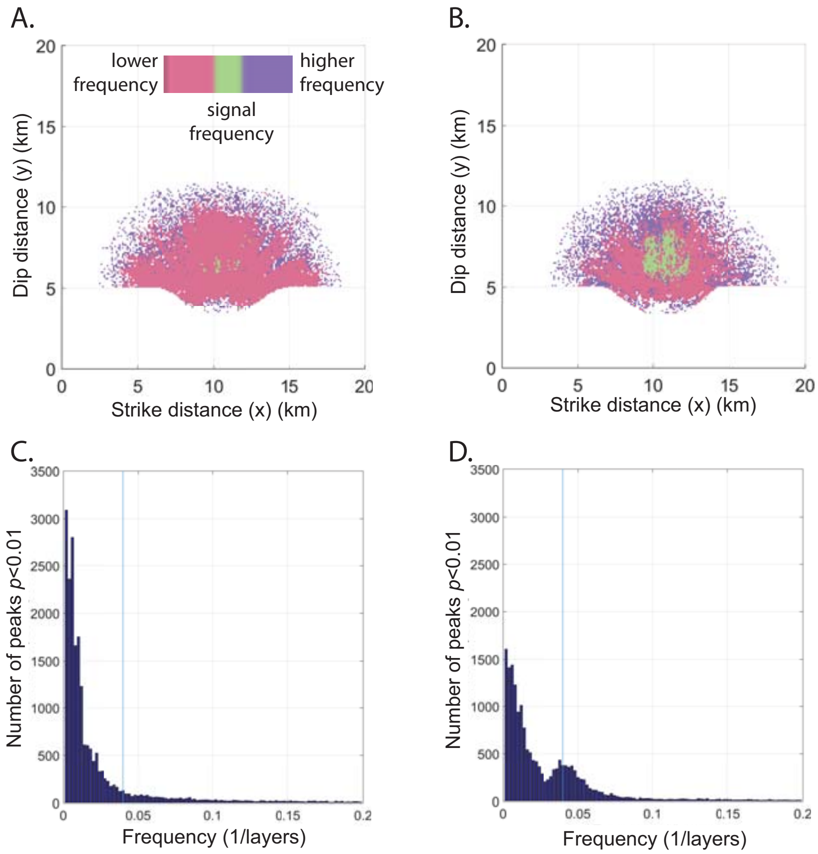

A.
B.
C.
D.
lower frequency
signal frequency
higher frequency
Dip distance (y) (km)
Strike distance (x) (km)
Number of peaks p<0.01
Frequency (1/layers)

Table 1 – Lobyte3D input parameters, typical values, and summary explanation .

Parameter	Unit	Typical values	Value used here	Description and rationale
$\rho_{\mathbf{a}}$	$kg \cdot m^{-3}$	1.225	1.225	Density of air, the ambient fluid for subaerial gravity flows.
$\rho_{\mathbf{w}}$	$kg \cdot m^{-3}$	$1.0 \cdot 10^{3}$	$1.0 \cdot 10^{3}$	Density of water, the ambient fluid for subaqueous gravity flows.
$\rho_{\mathbf{s}}$	$kg \cdot m^{-3}$	$2.6 \cdot 10^{3}$ - $2.7 \cdot 10^{3}$	$2.65 \cdot 10^{3}$	Density of the grains in a gravity flow, typically quartz or calcite.
$\mathbf{C_v}$		From 0 to 0.85	0.07	Sediment concentration (Mulder and Alexander, 2001)
$\boldsymbol{C_{vT}}$		0.1	0.1	Sediment concentration threshold separating low-concentration turbidity currents and high-concentration or hyperconcentrated gravity flows and debris flows (Mulder and Alexander, 2001)
$\boldsymbol{d_{50}}$	m	$0.25 \cdot 10^{-3}$	$0.25 \cdot 10^{-3}$	Mean grain diameter in each flow. Default value corresponds to a medium/fine sand mixture.
$\boldsymbol{U_{depos}}$	$m \cdot s^{-1}$	3.0	3.0	Threshold velocity for sediment deposition
FDF		From 0 to 20	10	Flow Dispersion Factor, controls flow dispersion, generating a wider or narrower and more elongate lobe deposit.
DTF		From 1.0 to -1.0	0	Deposit Thickness Factor, controls how the proportion of flow deposited in each destination cell changes during deposition, controlling lobe length and thickness distribution.

	Distance down dip (y) (km)	Number of beds	Max bed thickness (m)	Mean bed thickness (m)
Constant supply scenario	4	87	1.290	0.012
	5	336	0.752	0.023
	6	512	0.419	0.011
	7	498	0.133	0.003
	8	440	0.024	0.001
	9	347	0.005	0.000
	10	223	0.002	0.000
Oscillating supply scenario	4	85	1.116	0.012
	5	364	1.568	0.022
	6	573	0.330	0.009
	7	598	0.102	0.003
	8	516	0.035	0.001
	9	367	0.011	0.000
	10	181	0.005	0.000

Table 2. Bed statistics along a transect of vertical section locations (x=10km) for both model scenarios.